Available online at www.sciencedirect.com

ScienceDirect

Procedia Structural Integrity 24 (2019) 875–887

Structural Integrity Procedia

www.elsevier.com/locate/procedia

AIAS 2019 International Conference on Stress Analysis

Multiphysics numerical investigation on the aeroelastic stability of a Le Mans Prototype car

Corrado Groth[a], Andrea Chiappa[a], Stefano Porziani[a], Marco E. Biancolini[a,*], Emanuele Jacoboni[b], Elisa Serioli[b], Franco Mastroddi[c]

[a]*University of Rome "Tor Vergata", Department of Enterprise Engineering "Mario Lucertini", Via del Politecnico 1, Rome 00133, Italy*
[b]*Dallara, Via Provinciale 33, Varano de' Melegari 43040, Italy*
[c]*University of Rome "La Sapienza", Department of Mechanical and Aerospace Engineering, Via Eudossiana 18, Rome 00184, Italy*

Abstract

In the analysis and design of racing competition cars, numerical tools allow to investigate a wide range of solutions in short time and with high confidence in results. The great available computational power permits to combine simulation software so that different physics involved can be tackled at the same time. An important class of multi-physics simulations for motor sport addresses the fluid-structure interactions happening between the aerodynamic components of the car and the surrounding flow: this interaction can induce structural deformations and vibrations which, in turn, can influence the surrounding fluxes. In this paper, the flutter analysis of the front wing splitter mounted on the 2001 Le Mans Prototype car by Dallara (LMP1) is presented. The study was set up adopting high fidelity CAE models: a 400k shell elements FEM represents the full front wing assembly including the mounting frame, a 240M cells CFD represents the full car immersed in a box shaped wind tunnel. FEM extracted structural modal shapes are mapped onto the CFD mesh adopting Radial Basis Functions (RBF) mesh morphing so that the surfaces of the CFD model can be deformed according to retained modes. Such deformation is then propagated so that the volume mesh is adapted accordingly. The elastic CFD model with modes embedded was then loaded by applying a transient signal individually to each retained mode with a smoothed step function. A Reduced Order Model (ROM) for the aerodynamics of the coupled system was then extracted combining the results of the individual transient run. The critical speed experimentally observed to be in the operating range of the car was captured by the model quite well. The same workflow was then adopted to investigate a different design in which a stiffener has been introduced to increase the first mode natural frequency from 40Hz to 49.4Hz. Flutter speed was increased and moved outside the vehicle range. The car equipped with the improved part proved to perform on the track without previously detected instabilities.

Keywords: FSI; CFD; FEM; Flutter; Motorsport; ROM; RBF

* Corresponding author. Tel.: +39 0672597124.
E-mail address: biancolini@ing.uniroma2.it

10.1016/j.prostr.2020.02.077

1. Introduction

The study of the aeroelastic interaction between structural and fluid domains is gaining in the years more and more importance, driven primarily by the aeronautical industry in which this complex multiphysics phenomenon is of paramount importance. Aeronautical structures are indeed the result of extreme weight optimisation, translating in slender structures characterised by pronounced deformability and high sensitivity to Fluid-Structure Interaction (FSI). If, on one hand, engineers can take advantage from this strong multiphysics coupling by designing components that exploit the interaction between fluid and structure (such as reed valves and parachute canopies, in which FSI is the working principle of the mechanism itself), on the other one, dangerous phenomena that cannot be underestimated endangering structural integrity such as dynamic instabilities and flutter can occur. Given the relevance of the matter, several methods have been developed in the years to catch and simulate this phenomena faithfully, and an accurate determination of the transient aerodynamic load variation caused by structural displacements is still a challenge in the scientific community. The importance of providing the analyst with an advanced and accurate tool able to foresee and predict the behaviour of complex systems is justified by the risk posed to structural integrity, but also by the necessity of designing advanced and higher performance products. Historically the first numerical tools employed in aeroelasticity to evaluate the aerodynamic load variations due to unsteady boundary conditions have been the Doublet Lattice Method (DLM), Giesing et al. (1971), and the Morino Formulation (MF), Morino et al. (1975), in view of their excellent computational efficiency at the cost of an unavoidable simplification, introduced by linearizing the unsteady potential flow around a reference condition under a small perturbation hypothesis. The advent of massive computational power and the use of more efficient computer algorithms, allowed widespread adoption of more refined high fidelity numerical methods and tools relying on Computational Fluid Dynamics (CFD), removing the barriers introduced by analytical and simplified methods. Many efforts have been made in the last decades to improve existing numerical FSI methods, and several approaches are available in the literature. The most common, industrially employed high fidelity FSI approach, is the 2-way partitioned method foreseeing the mutual interaction between CFD and structural Finite Element Method (FEM) codes. Fluid dynamics and structural systems are kept segregated and solved separately in an iterative fashion, exchanging loads and displacements back and forth between the two solvers. While the possibility of employing commercial and closed source codes is a great advantage of this approach, significant drawbacks are emphasised both from a numerical and from an operative point of view, requiring several and complex data exchange processes. The loads acting on wetted surfaces must be indeed transferred from CFD to the FEM code in order to assess structural deformations, while nodal displacements have to be synchronised back to the fluid dynamic domain boundaries in order to evaluate the variation in the flow. This task is computationally intensive since numerical meshes are, generally, not matching for different solvers, and then a sophisticated mapping algorithms (Biancolini et al. (2018)) must be employed to transfer loads and displacements between both grids. Additional complexity is moreover introduced by the need of an appropriate algorithm to deform the CFD grid propagating displacements known at boundaries into the volume. The major bottleneck of this well validated method is the constant data transfer required, being mapping and mesh deformation needed at each iteration. This problem can be unbearable for unsteady simulations, in which mesh deformation and load mapping are carried at each time step when employing a weak coupling or at each inner iteration for strong coupling (Benra et al. (2011)). A powerful alternative, employed in this work, is the modal superposition method based on vibration theory (Di Domenico et al. (2018)). The degrees of freedom of the system are decreased by taking into account a Reduced Order Model (ROM) of the structure based on the first structural modal shapes obtained by means of the eigenvalue problem associated to the undamped structure (Castronovo et al. (2017)). Indeed, structural analysis is carried out only once to extract such shapes, and results in terms of displacements are imported in the CFD code to deform the numerical grid. A given structural deformation can be obtained as a linear superimposition of its modal shapes and modal forces can be computed by projecting the fluid dynamic pressures onto the modal shapes. For a generic FSI cycle the modal coordinates, and their derivatives for a transient simulation, can be computed as a function of the modal forces acting on the structure at each time step, but the opposite can be also done, by the fluid point of view, if the influence in terms of modal forces needs to be evaluated for a given imposed deformation. This is the case tackled in this paper, in which the aeroelastic stability of the Dallara LMP1 front wing splitter (Jacoboni et al. (2013)) was investigated by means of a flutter analysis. Modal shapes, computed by means of Altair Radioss™ were first imported in the CFD solver ANSYS® Fluent® using the Add On RBF Morph™, a commercial mesh morphing tool based on Radial Basis Functions (RBF). A transient run

was carried by exciting each mode of the deformable CFD model using a smoothed step function, computing the linearized aerodynamic transfer function matrix, dynamically relating the modal coordinates with the aerodynamic generalized forces, by using Scilab code. A flutter analysis was finally carried on the original and on a stiffened front wing splitter configuration by using the Newton-Raphson method on the generalized stability eigenproblem, catching the experimentally observed instabilities for the baseline geometry and demonstrating a flutter speed increase, moved outside a dangerous range, on the modified splitter. Favourable mathematical properties of RBF, such as smoothness and scalability, make them an appealing candidate for applications in several fileds: mesh morphing (De Boer et al. (2007)), geometrical modeling (Kojekine et al. (2003), Reuter et al. (2003)), shape optimization (Cella et al. (2017), Biancolini et al. (2014)) and adjoint filtering (Groth (2015)), to cite a few. A first application of the proposed ROM frequecy-domain linearization for the unsteady aerodynamic flutter analysis, with related assessment of the methodology, was introduced by Capri et al. (2006). FSI applications combining the present Reduced Order Methods and RBF can be found in literature (Castronovo et al. (2017)). The 2-way (Cella and Biancolini (2012), Keye (2009)) and the modal superposition (Biancolini et al. (2016), Andrejašič et al. (2016)) are also viable approaches for FSI static analyses. Van Zuijlen et al. (2007) showed a notable application of modal embedding for transient FSI using RBF on the AGARD 445.6 wing.

In the next sections the theoretical background on the aeroelastic system, the aerodynamic transfer function, flutter analysis and RBF will be introduced. The workflow employed for the Dallara SP1 analysis will be then shown together with testcase results.

2. Theoretical background

In this section a brief recall on the basic theory of the unsteady aerodynamics and its linearized ROM description (aerodynamic transfer function), the flutter problem and RBF theory is given.

2.1. Modelling the aeroelastic problem

The motion law governing the dynamic of a structural system can be easily obtained using the virtual work principle (Meirovitch (2001)). By approximating the generic displacement field $X(x,t)$ of the structure, function of space and time, using up to the n-th structural mode

$$X(x,t) = \sum_{i=0}^{n} N_i(x)\, q_i(t) \tag{1}$$

it is possible to reduce the partial differential equation of motion to an ordinary differential equation in which each modal degree of freedom (DOF) $q_i(t)$ can be solved separately thanks to the orthogonal property of structural eigenvectors $N_i(x)$. The resulting equation of motion can be written as:

$$[M]\{\ddot{q}(t)\} + [C]\{\dot{q}(t)\} + [K]\{q(t)\} = \{Q(t)\} \tag{2}$$

where $\{q(t)\}$ is the vector having as components the i modal coordinates, $[M], [C]$, and $[K]$ are respectively the diagonal mass, damping and stiffness matrices and $\{Q\}$ is the modal force or Generalized Aerodynamic Forces (GAF) vector obtained projecting the fluid dynamic loads on each modal shape. Moving from time to Laplace domain (with s Laplace variable), equation 2 can be rewritten as

$$\left([M]\, s^2 + [C]\, s + [K]\right)\{q(s)\} = \{Q(s)\} \tag{3}$$

in which $\{q(s)\}$ and $\{Q(s)\}$ are the Laplace transforms of $\{q(t)\}$ and $\{Q(t)\}$. Equation 3 can be rewritten by assuming the hypothesis of linearized aerodynamics, by expressing the generalized aerodynamic forces in Laplace domain as functions of the modal coordinates vector by introducing the GAF transfer function matrix $[H(p)]$ such that:

$$\{Q(s)\} = q_\infty [H(p)] \{q(s)\} \tag{4}$$

where the aerodynamic transfer function was written as function of the reduced Laplace variable $p := sL_a/V_\infty$, function of the reference length and velocity, and q_∞ is the dynamic pressure. In order to evaluate the linearized aerodynamic operator in terms of GAF transfer-function matrix, it is possible to employ a CFD method, similarly to what done in a wind tunnel experimental campaign, by carring a series of different numerical simulations (see Capri et al. (2006)). Indeed, the matrix $[H(p)]$ expresses the linearized link between generalized displacements and generalized aerodynamic forces in the case of small perturbations. This implies the possibility of building the GAF matrix by evaluating –via CFD simulations- ouput/input ratios between aerodynamic modal loads and modal displacements. Indeed, the first step is to obtain a stationary equilibrium between the structural and fluid dynamic systems, for example employing the static modal superposition method (Groth et al. (2019)) to reach a trimmed starting configuration used as a reference for the linearization of aerodynamic loads. Starting from this configuration, it is then possible to evaluate, via CFD simulations, the unsteady variation of the generalized load vector $\{Q(t)\}^{(i)}$ when a moving time law is assigned to the (i)-th modal degree of freedom by tweaking the modal coordinate $q(t)_i$. By exciting only the (i)-th modal shape, the (i)-th aerodynamic transfer matrix column can be computed as the ratio relationship between the Fourier transform of the vector $\{Q(t)\}^{(i)}$ and the Fourier of the modal input signal applied to the aerodynamic system $q(t)_i$. Thus, the i-th column of the GAF frequency response matrix can be estimated as:

$$[H(\omega; V_\infty)|_i] = \frac{\mathcal{F}\left(\{Q(t)\}^{(i)}\right)}{\mathcal{F}\left(q(t)_i\right)} \tag{5}$$

where $\mathcal{F}(\cdot)$ is the Fourier transform that can be efficiently performed as a Fast Fourier Transform (FFT) on the finite discrete numerical problem. Note that the identified linearized operator is defined as function of the frequency domain variable ω and it is also parametrically dependent by the flow speed simulation V_∞; however, this double dependency can be standarly compacted as a dependency on the unique undimensional reduced frequency $k := \omega L_a/V_\infty$. Repeating this simulation procedure for all the modal DOFs and mounting the columns into a unique matrix, the GAF matrix is is achieved in Fourier domain and its Laplace domain counterpart (namely, the GAF transfer function matrix) can be obtained just substituting the Fourier variable $j\omega$ with the Laplace variable s (see Eq. 3).

2.2. Time input for building the aerodynamic ROM

For what said on the previous section, the great efficiency of the method employed in this work is given by the fact that only a single steady FSI study must be carried in order to achieve the trimmed configuration, after which each mode shape is excited with a prescribed time law and the system response is employed to evaluate the GAF frequency response matrix. Choosing a proper time law of motion to be prescribed to each degree of freedom is however not a trivial task. Applied displacements have indeed to excite reduced frequencies in the range of interest, with an amplitude big enough to stand above numerical noise but small enough to comply with the assumption of small displacements. Several choices (Romanelli and Serioli (2007)) can be made in terms of temporal laws to be applied to the vector of modal coordinates, such as the harmonic, impulsive and step functions. In this work a smoothed step function was employed to remove the problems linked with the discontinuities of a plain step function. Using a smoothed step function it is also possible to use a larger temporal discretization with respect to an impulsive function to correctly catch the fluid dynamic transient response.

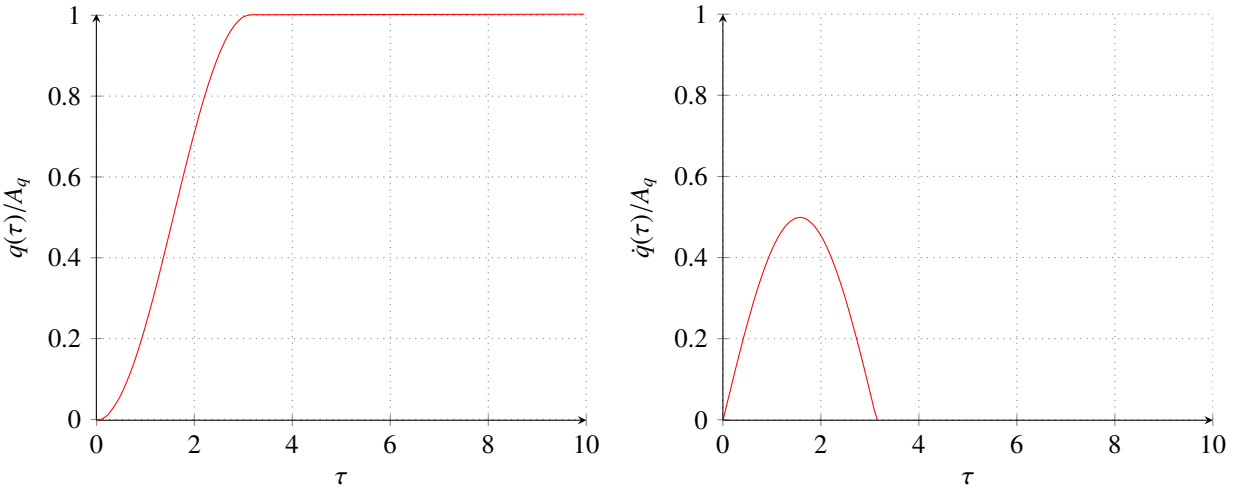

Fig. 1: generalized displacement and velocity for a generic smoothed step function

System input needs to excite frequencies inside the chosen range $k = [0, k_{max}]$, with a maximum amplitude computed, for each DOF, in function of the maximum modal displacement d_{max}:

$$A_q = \frac{4\epsilon L_a}{d_{max} k_{max}} \tag{6}$$

Choosing $\epsilon = \tan(1\,\text{deg})$ so to obtain a small modal velocity compared to the reference velocity, and using the dimensionless time $\tau = tV_\infty / L_a$ the smoothed step function can be written as:

$$q_i(\tau) = \begin{cases} \frac{A_q}{2} \cdot \left[1 - \cos\left(k_q \tau\right)\right] & \text{if } \tau < \tau_q \\ A_q & \text{if } \tau \geq \tau_q \end{cases} \tag{7}$$

The resulting generalized velocity is:

$$\dot{q}_i(\tau) = \begin{cases} \frac{A_q k_q V_\infty}{2L_a} \cdot \left[1 - \sin\left(k_q \tau\right)\right] & \text{if } \tau < \tau_q \\ 0 & \text{if } \tau \geq \tau_q \end{cases} \tag{8}$$

In figure 1 the generalized displacement and velocity applied using a generic smoothed step function are shown with respect to the dimensionless time τ

2.3. Radial Basis Functions mesh morphing

RBF are mathematical interpolation functions able to retrieve, on a distance basis, scalar information known at source points, i.e. a cloud of discrete points supposed to be the input of the problem. The interpolation shape between source points can be controlled by selecting an appropriate radial function and by defining the kind of support it guarantees (local or global), meaning the domain in which the function is not zero valued (De Boer et al. (2007)).

Some of the most common functions are shown in table 1. RBF can be defined in generic n dimensional spaces and are function of the distance that, in the case of morphing, can be assumed as the euclidean norm of the distance between two points in the space. To define in full the RBF starting from passage information at source points, a

Table 1: Common RBF with global and local support.

Compactly supported RBF	Abbreviation	$\phi(\zeta)$
Wendland C^0	$C0$	$(1-\epsilon\zeta)^2$
Wendland C^2	$C2$	$(1-\epsilon\zeta)^4(4\epsilon\zeta+1)$
Wendland C^4	C4	$(1-\epsilon\zeta)^6(\frac{35}{3}\epsilon\zeta^2+6\epsilon\zeta+1)$
Globally supported RBF	**Abbreviation**	$\phi(\zeta)$
Polyharmonic spline	PHS	r^n, n odd $r^n log(r)$, n even
Thin plate spline	TPS	$r^2 log(r)$
Multiquadric biharmonics	MQB	$\sqrt{a^2+(\epsilon r)^2}$
Inverse multiquadric biharmonics	IMQB	$\frac{1}{\sqrt{a^2+(\epsilon r)^2}}$
Quadric biharmonics	QB	$1+(\epsilon r)^2$
Inverse quadric biharmonics	IQB	$\frac{1}{1+(\epsilon r)^2}$
Gaussian biharmonics	GS	$e^{-\epsilon r^2}$

linear problem (Buhmann (2000)) must be solved in order to find system coefficients. Once the coefficients have been found the function at a given node of the mesh, being it inside (interpolation) or outside the domain (extrapolation), can be calculated according the radial summation centered at the probe position. Adopting such interpolation for the components of a deformation field it is then possible to define at known points the displacement in the space and then to retrieve it at mesh nodes, obtaining a mesh deformation that leaves unaltered the grid topology (Beckert and Wendland (2001), Biancolini (2012)).

The interpolation function is composed by the radial function ϕ and, in some situations, by a polynomial term h with a degree that depends on the kind of the chosen radial function which is added to assure uniqueness of the problem. If N is the total number of source points it can be written:

$$s(\mathbf{x}) = \sum_{i=1}^{N} \gamma_i \phi(\|\mathbf{x} - \mathbf{x}_{k_i}\|) + h(\mathbf{x}) \tag{9}$$

The passage of the RBF through source points and the imposing orthogonality conditions for the polynomial terms:

$$s(\mathbf{x}_{k_i}) = g_i, 1 \le i \le N \qquad \text{and} \qquad \sum_{i=1}^{N} \gamma_i p(\mathbf{x}_{k_i}) = 0 \tag{10}$$

for all the polynomials p of degree less or equal to polynomial h. A single interpolant exists if the basis is conditionally positive definite (Micchelli (1986)). If the degree is $m \le 2$ (Beckert and Wendland (2001)) a linear polynomial can be

used:

$$h(\mathbf{x}) = \beta_1 + \beta_2 x_1 + \beta_3 x_2 + ... + \beta_{n+1} x_n \tag{11}$$

The system 10 built to calculate coefficients and weights can be easily written in matrix form for an easy implementation:

$$\begin{bmatrix} \mathbf{M} & \mathbf{P} \\ \mathbf{P}^T & \mathbf{0} \end{bmatrix} \begin{Bmatrix} \boldsymbol{\gamma} \\ \boldsymbol{\beta} \end{Bmatrix} = \begin{Bmatrix} \mathbf{g} \\ \mathbf{0} \end{Bmatrix} \tag{12}$$

Where $\mathbf{g}$ is is the vector of known terms for each source point and $\mathbf{M}$ is the interpolation matrix with the radial function transformed distances between source points:

$$M_{ij} = \phi(\|\mathbf{x}_{k_i} - \mathbf{x}_{k_j}\|), 1 \leq i \leq N, 1 \leq j \leq N \tag{13}$$

$\mathbf{P}$ is the constraint matrix resulting from the orthogonality conditions:

$$\mathbf{P} = \begin{pmatrix} 1 & x_{k_1} & y_{k_1} & z_{k_1} \\ 1 & x_{k_2} & y_{k_2} & z_{k_2} \\ \vdots & \vdots & \vdots & \\ 1 & x_{k_N} & y_{k_N} & z_{k_N} \end{pmatrix} \tag{14}$$

The system 12 is solved considering as known terms the three components of the deformation field. Once the RBF weights and polynomial coefficients of the system have been obtained, displacement values for the three directions can be obtained at a given $\mathbf{x}$ point as:

$$\begin{cases} S_x(\mathbf{x}) = \sum_{i=1}^{N} \gamma_i^x \phi(\|\mathbf{x} - \mathbf{x}_{k_i}\|) + \beta_1^x + \beta_2^x x_1 + \beta_3^x x_2 + \beta_4^x x_n \\ S_y(\mathbf{x}) = \sum_{i=1}^{N} \gamma_i^y \phi(\|\mathbf{x} - \mathbf{x}_{k_i}\|) + \beta_1^y + \beta_2^y x_1 + \beta_3^y x_2 + \beta_4^y x_n \\ S_z(\mathbf{x}) = \sum_{i=1}^{N} \gamma_i^z \phi(\|\mathbf{x} - \mathbf{x}_{k_i}\|) + \beta_1^z + \beta_2^z x_1 + \beta_3^z x_2 + \beta_4^z x_n \end{cases} \tag{15}$$

2.4. Flutter analysis

From a Physical point of view the Flutter problem can be considered as a dynamic instability caused by self excited divergent oscillations and can be seen as a positive feedback between body deflections and fluid dynamic loads. From a mathematical point of view instead, the Flutter analysis of an aeroelastic system can be considered as the instability study of its linearized and time-invariant system under the hypothesis of small perturbations around an equilibrium conditions. In the case taken into account in this work the equilibrium condition is the trimmed configuration obtained as a result of the static FSI problem.

Recalling equation 3, and splitting the load term into two separate contributions to take into account the steady loads ensuring the equilibrium trimmed configuration and the unsteady aerodynamic loads describing the dynamic around the steady solution, the linearized flutter problem consider only the latter as given by Eq. 4. Thus, for a given value of the flight speed, V_∞, the flutter stability problem consists of determining the pole S and the associated eigen-vector

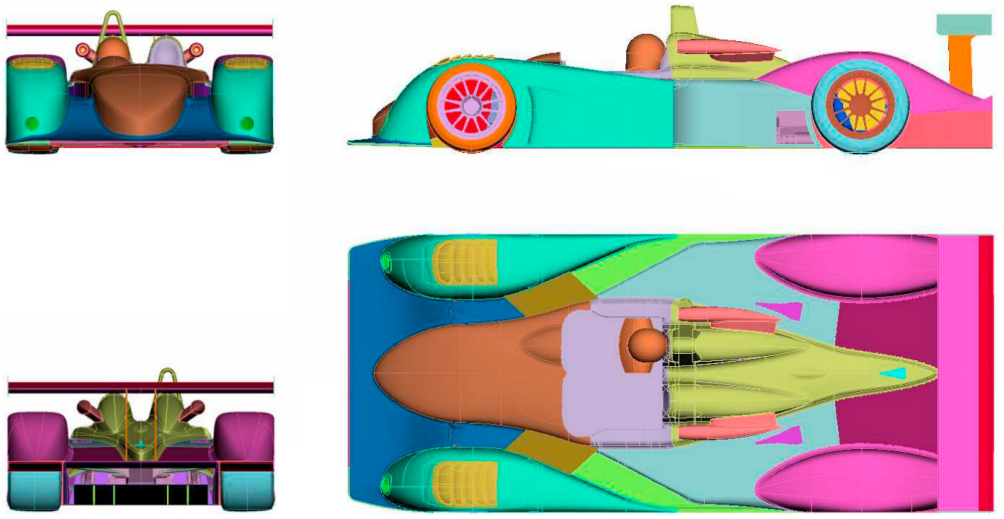

Fig. 2: LMP1 geometry analized in this work

$\{w\}$ ($n+1$ unknowns) satisfying the following n algebraic equations:

$$\left([M]\, s^S + [C]\, s + [K] - \frac{1}{2}\varrho_\infty V_\infty^2\, [H(s; V_\infty)]\right)\{w\} = 0 \tag{16}$$

which can be rewritten in the form

$$[F(s, V_\infty)]\,\{w\} = 0 \tag{17}$$

System 16 however cannot be solved alone, since it is equal to the solution of n equations in $n+1$ unknown. A normalization for the eigenvector $\{w\}$ is then added so having the following final nonlinear system of $n+1$ equations in the n (components of $\{w\}$) $+1$ (the pole s)

$$\begin{aligned} &[F(s, V_\infty)]\,\{w\} = 0 \\ &\{w\}^T\,[W]\,\{w\} = c \end{aligned} \tag{18}$$

where $[W]$ is a diagonal weight matrix and c is an arbitrary constant fixing the eigenvector magnitude. This non linear system can be solved using an iterative solver such as Newton Raphson method.

3. Application

In this section, the flutter analysis carried on the front wing splitter mounted on the 2001 Le Mans Prototype car by Dallara (LMP1) is presented. This study was born from what found during a test drive in which the driver, at a given velocity, felt an irregular behaviour of the front assembly ascribable to a flutter instability of the front wing. The solution found on the track was to add a stiffening spider, increasing the modal frequencies of the whole assembly and shifting the flutter velocity outside the vehicle range. In this work the validation of that shape modification will be given by investigating baseline and modified geometries.

In figure 2 the geometry of the Dallara LMP1 car, employed in this work, is shown. For what said in the previous paragraphs, the flow around the vehicle was investigated taking into account the whole geometry, but only the front wing portion, shown in figure 3, was used for the FSI study as wetted surface.

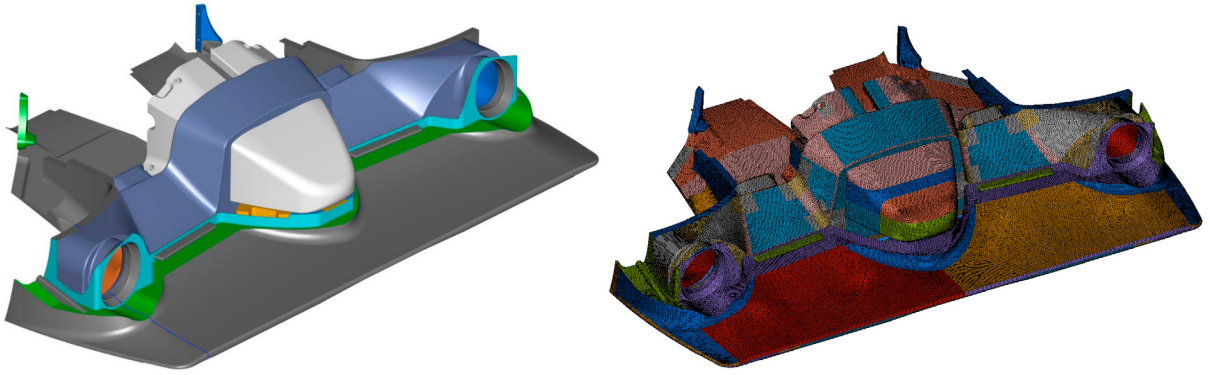

Fig. 3: LMP1 front wing employed for eigenvalue analysis. Left: geometry, right: FEM mesh

The structural eigenvalue problem was solved for both the baseline and modified geometries adopting a FEM model comprised of about 400k shell elements. Results in terms of modal shapes and frequencies are shown in figure 4, in which the first four modal shapes are shown in the top row for the original geometry and in the bottom row for the front wing assembly stiffened using the spider.

As expected the frequencies on the updated model have been shifted up thanks to the higher stiffness introduced by the spider structure. The first two modal shapes appear very similar between the two models and to better investigate the differences in terms of modal shapes the Modal Assurance Criterion (MAC) was employed.

In table 2 the results of the MAC between baseline and updated models are shown, and the previously noticed similarity is confirmed by the high correlation numbers for the first two modes, highlighted in green. The addition of the spider introduced a significant variation for modes three and four that have a very low MAC number.

The CFD analysis, conducted using a $k-\epsilon$ realizable turbulence model and considering the air uncompressible, was carried for different velocities ranging from 40 m/s to 100 m/s. To accelerate the CFD evaluation a half-vehicle symmetric domain comprised of about 240M cells was employed, considering a driver in both seats.

In figure 5 the contours of the pressure coefficient are shown for the 50 m/s flow velocity at the inlet.

Transient runs were carried for each velocity inlet by exciting in turn the modal shapes shown in figure 4 using the smoothed step functions described in the previous paragraphs, achieving the GAF matrix. The flutter analysis on the baseline configuration was carried employing the Newton Raphson method as explained in the previous paragraph,

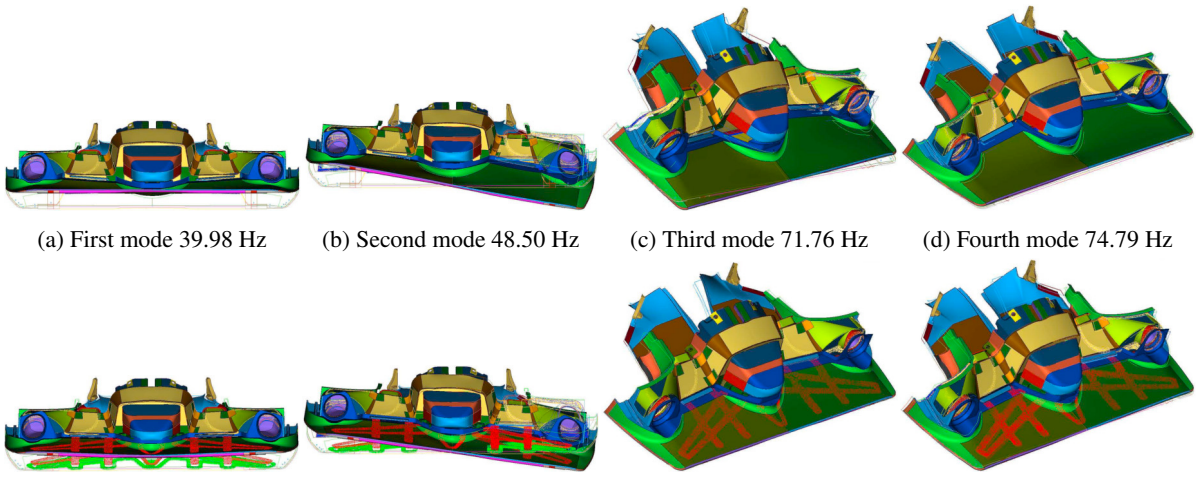

(a) First mode 39.98 Hz (b) Second mode 48.50 Hz (c) Third mode 71.76 Hz (d) Fourth mode 74.79 Hz

(e) First mode 49.40 Hz (f) Second mode 53.89 Hz (g) Third mode 79.50 Hz (h) Fourth mode 81.77 Hz

Fig. 4: First four modal shapes for the baseline geometry (top row) and updated geometry (bottom row)

Table 2: MAC table for the front wing assembly

	Baseline			
Updated	0.915	0.379	0.082	0.300
	0.397	0.982	0.102	0.343
	0.494	0.503	0.135	0.445
	0.574	0.540	0.158	0.492

using cubic splines to interpolate the Aerodynamic matrix known at discrete velocities and reduced frequencies. This analysis confirms a flutter instability. By plotting the norm g of the Real and Imaginary parts of the complex pole $s = \mathcal{R}e(s) + j\mathcal{I}mag(s) = g\,2\pi f + j2\pi f$ with respect to the velocity V, it is possible to highlight the crossing of g on the positive semi-plane. V - f and V - g diagrams are shown in figure 6. The critical velocity obtained for the baseline geometry is 47.6 m/s with a frequency of 65.7 Hz.

Similar remarks can be done by examining the results, obtained with the stiffened configuration, employing the first four vibrational modes. Also in this case the first mode is responsible for the instabilities, occurring at 68.1 m/s and at a frequency of 73.1 Hz. In figure 7 the V - f and V - g diagrams are shown, highlighting the instability mainly associated to the first assumed mode shape.

Considering the reached flutter condition with flutter frequency ω_{cr} and flutter speed V_{cr}, the (four) components of the related critical eigenvector $\{w_{cr}\}^T = \{w_{1_{cr}}, w_{2_{cr}}, w_{3_{cr}}, w_{4_{cr}}\}$ can be evaluated by the omogeneous problem

$$\left(-\omega_{cr}^2\,[M] + [K] - \frac{1}{2}\rho V_{cr}^2\,[H(\omega_{cr}, V_{cr})]\right)\begin{Bmatrix} w_1^{cr} \\ w_2^{cr} \\ w_3^{cr} \\ w_4^{cr} \end{Bmatrix} = 0 \tag{19}$$

These four numbers are able to quantify the participation of each structural modes to the flutter critical vibration: in this case a considerable value obtained for the component $w_{1_{cr}}$ has indicated the first structural mode as the main one involved in the flutter vibration.

In figure 8 the flutter deformation for the stiffened geometry is shown amplified 300 times.

4. Conclusions

In this paper the flutter analysis of the front wing splitter mounted on the 2001 Le Mans Prototype car by Dallara (LMP1) was presented. By using high fidelity fluid dynamic and structural models, a modal superposition coupling was employed using Radial Basis Functions (RBF) morphing. The vibration modes of the baseline front wing, and of a similar model stiffened using a spider structure, were excited employing a finely-tuned smoothed step function, carrying transient CFD simulations in order to build a suitable linearized unsteady ROM for aerodynamics. Thus,

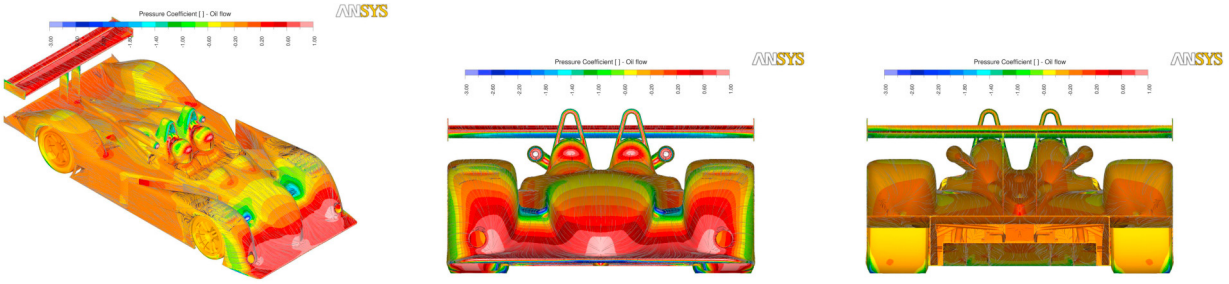

Fig. 5: LMP1 Pressure coefficient contours for the 50 m/s case

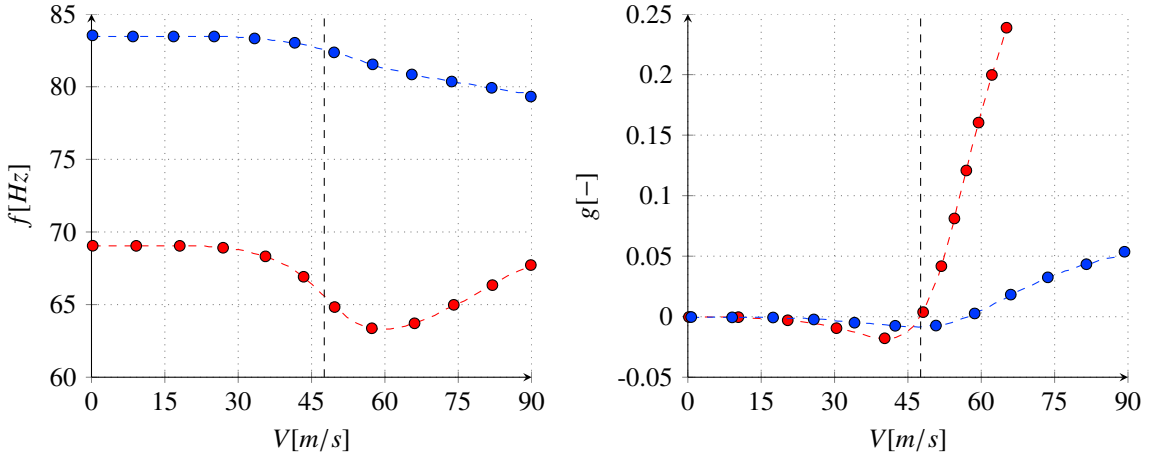

Fig. 6: V - f and V - g diagrams for the baseline geometry. mode 1, mode 2.

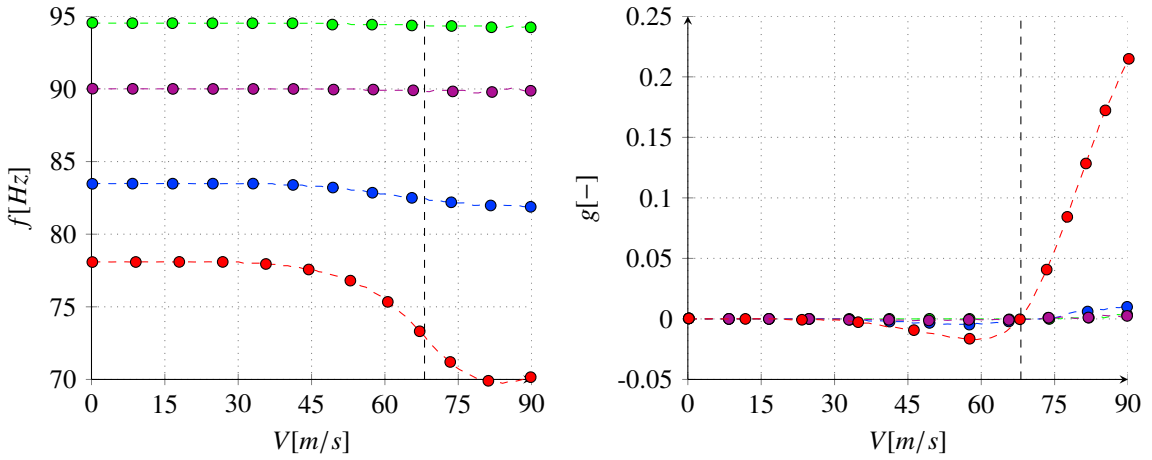

Fig. 7: V - f and V - g diagrams for the stiffened geometry. mode 1, mode 2, mode 3, mode 4.

aerodynamic transfer function matrices were built for both the original and the stiffened models, using the nonlinear method to solve the flutter problem. The critical speed experimentally observed to be in the operating range of the car was satisfactorily captured by the model, underestimating of 13.9 m/s both the baseline and the reinforced structures. This difference could be ascribable to a structural model not detailed enough, especially for what is concerned by the structural model constraints, and for a simplification adopted in the transient fluid dynamic simulations in which the front wheels were removed to accelerate the CFD calculation.

References

Andrejašič, M., Eržen, D., Costa, E., Porziani, S., Biancolini, M., Groth, C., 2016. A mesh morphing based FSI method used in aeronautical optimization applications, in: ECCOMAS Congress 2016 - Proceedings of the 7th European Congress on Computational Methods in Applied Sciences and Engineering.

Beckert, A., Wendland, H., 2001. Multivariate interpolation for fluid-structure-interaction problems using radial basis functions. Aerospace Science and Technology 5, 125–134. doi:10.1016/S1270-9638(00)01087-7.

Benra, F.K., Dohmen, H.J., Pei, J., Schuster, S., Wan, B., 2011. A comparison of one-way and two-way coupling methods for numerical analysis of fluid-structure interactions. Journal of Applied Mathematics 2011. doi:10.1155/2011/853560.

Biancolini, M., Cella, U., Groth, C., Genta, M., 2016. Static Aeroelastic Analysis of an Aircraft Wind-Tunnel Model by Means of Modal RBF Mesh Updating. Journal of Aerospace Engineering 29. doi:10.1061/(ASCE)AS.1943-5525.0000627.

Biancolini, M., Chiappa, A., Giorgetti, F., Groth, C., Cella, U., Salvini, P., 2018. A balanced load mapping method based on radial basis functions and fuzzy sets. International Journal for Numerical Methods in Engineering 115, 1411–1429.

Biancolini, M., Viola, I., Riotte, M., 2014. Sails trim optimisation using CFD and RBF mesh morphing. Computers & Fluids 93, 46–60. URL: http://linkinghub.elsevier.com/retrieve/pii/S0045793014000140, doi:10.1016/j.compfluid.2014.01.007.

Biancolini, M.E., 2012. Mesh Morphing and Smoothing by Means of Radial Basis Functions (RBF), in: Handbook of Research on Computational Science and Engineering. IGI Global. volume I, pp. 347–380. doi:10.4018/978-1-61350-116-0.ch015.

Buhmann, M.D., 2000. Radial basis functions. Acta Numerica 2000 9, S0962492900000015. doi:10.1017/S0962492900000015.

Capri, F., Mastroddi, F., Pizzicaroli, A., 2006. A Linearized Aeroelastic Analysis for a Launch Vehicle in Transonic Flow. AIAA - Journal Spacecraft and Rockets 43, 92–104. doi:10.2514/1.13867.

Castronovo, P., Mastroddi, F., Stella, F., Biancolini, M.E., 2017. Assessment and development of a ROM for linearized aeroelastic analyses of aerospace vehicles. CEAS Aeronautical Journal 8, 353–369. URL: http://link.springer.com/10.1007/s13272-017-0243-6, doi:10.1007/s13272-017-0243-6.

Cella, U., Biancolini, M.E., 2012. Aeroelastic Analysis of Aircraft Wind-Tunnel Model Coupling Structural and Fluid Dynamic Codes. Journal of Aircraft 49, 407–414. URL: http://arc.aiaa.org/doi/abs/10.2514/1.C031293, doi:10.2514/1.C031293.

Cella, U., Groth, C., Biancolini, M., 2017. Geometric parameterization strategies for shape optimization using RBF mesh morphing. doi:10.1007/978331945781954.

De Boer, A., van der Schoot, M.S., Bijl, H., 2007. Mesh deformation based on radial basis function interpolation. Computers and Structures 85, 784–795. doi:10.1016/j.compstruc.2007.01.013.

Di Domenico, N., Groth, C., Wade, A., Berg, T., Biancolini, M., 2018. Fluid structure interaction analysis: vortex shedding induced vibrations. Procedia Structural Integrity 8, 422–432. URL: https://doi.org/10.1016/j.prostr.2017.12.042http://linkinghub.elsevier.com/retrieve/pii/S2452321617305358, doi:10.1016/j.prostr.2017.12.042.

Giesing, J., Kalman, T., Rodden, W., 1971. Direct application of the non planar Doublet-Lattice method. Technical Report. AFFDL. AFFDL-TR-71-5, part I Vol. I and II.

Groth, C., 2015. Adjoint-based shape optimization workflows using RBF. Ph.d thesis. University of Rome Tor Vergata. doi:10.13140/RG.2.2.33913.06245.

Groth, C., Cella, U., Costa, E., Biancolini, M., 2019. Fast high fidelity cfd/csm fluid structure interaction using rbf mesh morphing and modal superposition method. Aircraft Engineering and Aerospace Technology URL: https://www.scopus.com/inward/record.uri?eid=2-s2.0-85064015261&doi=10.1108%2fAEAT-09-2018-0246&partnerID=40&md5=4c6e2f39a42059f64b9b8f5b99dc0175, doi:10.1108/AEAT-09-2018-0246. cited By 0.

Jacoboni, E., Mastroddi, F., Serioli, E., 2013. Studio della stabilità aeroelastica di una vettura prototipo Le Mans LMP2.

Keye, S., 2009. Fluid-Structure-Coupled Analysis of a Transport Aircraft and Comparison to Flight Data, in: 39th AIAA Fluid Dynamics Conference, American Institute of Aeronautics and Astronautics, Reston, Virigina. URL: http://arc.aiaa.org/doi/10.2514/6.2009-4198, doi:10.2514/6.2009-4198.

Kojekine, N., Hagiwara, I., Savchenko, V., 2003. Software tools using CSRBFs for processing scattered data. Computers and Graphics (Pergamon)

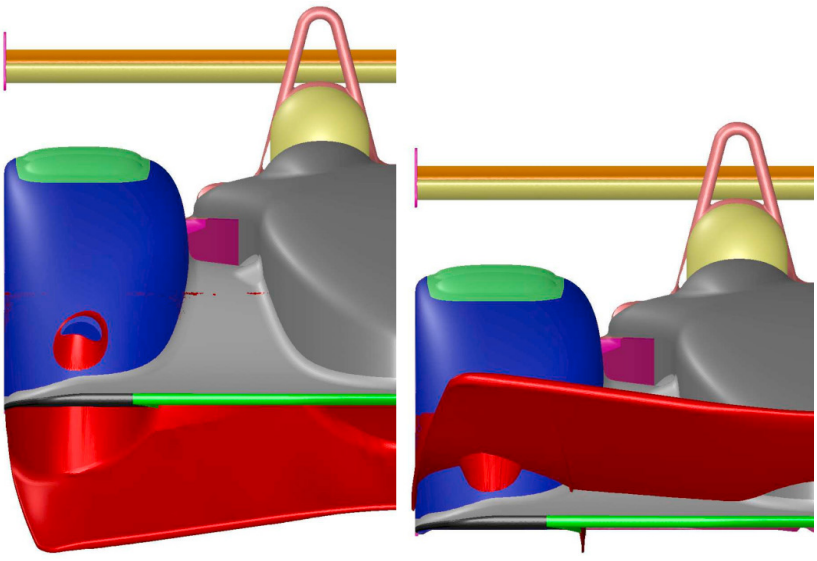

Fig. 8: LMP1 Flutter mode deformation, amplified 300 times

27, 311–319. doi:10.1016/S0097-8493(02)00287-X.

Meirovitch, L., 2001. Fundamentals of Vibrations. McGraw-Hill higher education, McGraw-Hill. URL: https://books.google.it/books?id=u358QgAACAAJ.

Micchelli, C.A., 1986. Interpolation of scattered data: Distance matrices and conditionally positive definite functions. Constructive Approximation 2, 11–22. doi:10.1007/BF01893414.

Morino, L., Chen, L., Suciu, E., 1975. Steady and Oscillatory Subsonic and Supersonic Aerodynamic around Complex Configuration. AIAA Journal 13, 368–374. doi:10.2514/3.49706.

Reuter, P., Tobor, I., Schlick, C., Dedieu, S., 2003. Point-based modelling and rendering using radial basis functions. Proceedings of the 1st international conference on Computer graphics and interactive techniques in Austalasia and South East Asia - GRAPHITE '03 , 111doi:10.1145/604471.604494.

Romanelli, G., Serioli, E., 2007. Un approccio libero alla moderna elasticità strutturale.

Van Zuijlen, A., De Boer, A., Bijl, H., 2007. Higher-order time integration through smooth mesh deformation for 3D fluidstructure interaction simulations. Journal of Computational Physics 224, 414–430. URL: http://linkinghub.elsevier.com/retrieve/pii/S002199910700143X, doi:10.1016/j.jcp.2007.03.024.